

WegCenter/UniGraz Technical Report for FFG-ALR No. 4/2007

FFG-ALR Study:

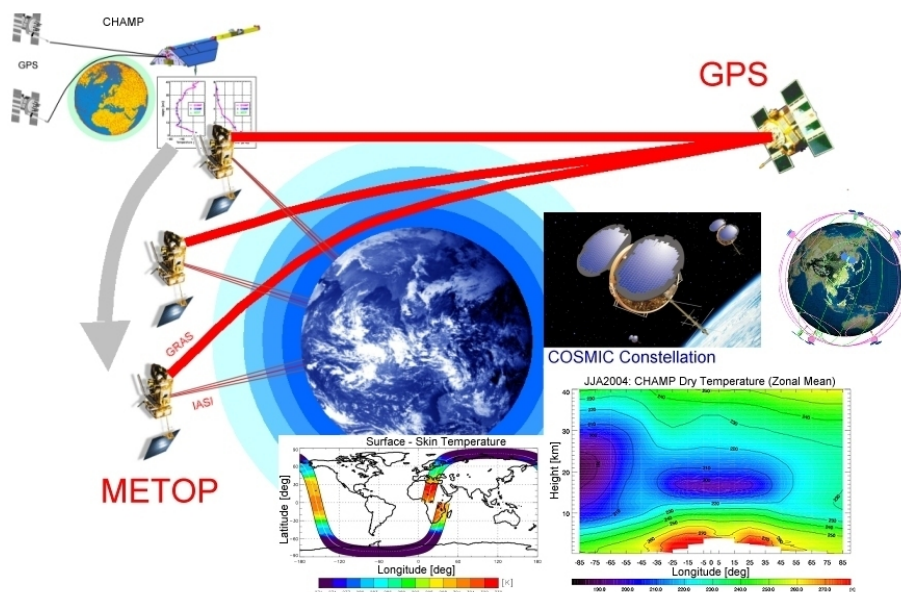
MULTICLIM – From CHAMP towards Multi-Satellite Climate
Monitoring based on the METOP and COSMIC Missions
[Contract No: ALR-OEWP-WV-326/06 – March 2006]

VALIDATION REPORT

Initial validation of atmospheric profiles and SST retrieved from MetOp IASI data and preparation of climatology processing

M. Schwaerz, M. Pock, B. Pirscher, and G. Kirchengast

Wegener Center for Climate and Global Change (WegCenter),
University of Graz, Graz, Austria



November 2007

Contents

List of Acronyms	v
1 Introduction	1
2 Validation of Atmospheric Profiles and SST from MetOp IASI	3
2.1 Validation Setup and Validation Datasets	3
2.1.1 Advanced Infrared Sounding with the MetOp IASI Sensor	3
2.1.2 IASI Test Orbit Data and ECMWF Reference Data	4
2.1.3 Validation Methodology	4
2.2 Temperature, Humidity, Ozone, and SST Validation	5
2.2.1 Validating Temperature, Humidity, and Ozone Profile Retrievals	5
2.2.2 Validating Sea Surface Temperature (SST) Retrievals	6
2.3 Channel Selection Methods and Single-Parameter Retrieval Assessment	6
2.3.1 Comparison of Information-Content and Maximum-Sensitivity Channel Selection	6
2.3.2 Comparison of Joint Multi-Parameter Retrieval to Single-Parameter Retrieval	8
3 Preparation of Climatology Processing	19
3.1 Grid Definitions and the Climatology Processing System (CLIPS)	19
3.1.1 Climatological Averaging Grid Definition, Datasets, and Example Season	19
3.1.2 Overview of the Climatology Processing System CLIPS	19
3.2 High-Resolution and Zonal-Band Climatology Processing Demonstration	21
3.2.1 Demonstration of Latitude-Altitude Climatological Resolution	21
3.2.2 Demonstration of Horizontal (Latitude-Longitude) Climatological Resolution	21
3.2.3 Demonstration of Zonal-Band Climatological Resolution	21
4 Conclusions and Outlook	27
Acknowledgments	28
List of References	29

List of Abbreviations

Acronym	Description
CIRA	COSPAR International Reference Atmosphere
COSPAR	Committee on Space Research
CNES	Centre National d'Etudes Spatial
CPU	Central Processing Unit
ECMWF	European Centre for Medium-Range Weather Forecasts
EGOPS	End-to-end GNSS Occultation Performance Simulator
ENVISAT	Environmental Satellite
ESA	European Space Agency
EUMETSAT	European Organisation for the Exploitation of Meteorological Satellites
FTC	Fast Transmittance Coefficient
FWHM	Full Width at Half Maximum
GNSS	Global Navigation Satellite System
GPS	Global Positioning System
IASI	Infrared Atmospheric Sounding Interferometer
IC	Information Content
IR	Infrared
ISRF	Instrument Spectral Response Function
METOP	Meteorological Operational (Satellite)
MS	Maximum Sensitivity
NWP	Numerical Weather Prediction
pdf	probability density function
RMS	Root Mean Square
RO	Radio Occultation
RT	Radiative Transfer
RTIASI	Radiative Transfer Model for IASI
SAT	Surface Air Temperature (2 m Temperature)
SNR	Signal-to-noise Ratio
SST	Surface Skin Temperature; Sea Surface Temperature
UTC	Coordinated Universal Time

Table 1: The Table contains the relevant acronyms used in the current work.

1 Introduction

The overarching goal of MULTICLIM is to prepare for global monitoring of the climate evolution of the upper troposphere/lower stratosphere region with unprecedented accuracy and consistency and thereby help to improve the ability to detect, attribute, and predict climate variability and change. The key datasets for this purpose are RO data and IASI interferometer data, of which the latter are in the focus of the MULTICLIM project.

The IASI (Infrared Atmospheric Sounding Interferometer – see, e.g. *Camy-Peyret and Eyre* (1998), *Weisz* (2001), <http://smc.cnes.fr/IASI/>) instrument is part of the core payload of the MetOp series of polar-orbiting operational meteorological satellites currently prepared for EU-METSAT where the first satellite, MetOp-A was successfully launched on Oct. 19, 2006. IASI is a Michelson-type Fourier transform interferometer which samples a part of the infrared (IR) spectrum contiguously from 645 cm^{-1} to 2760 cm^{-1} ($\sim 3.6\text{ }\mu\text{m}$ - $15.5\text{ }\mu\text{m}$) with an unapodized spectral resolution of about 0.5 cm^{-1} .

The project aims at advancing IASI retrieval algorithms and at preparing IASI climatology processing for climatologies at high horizontal resolution, but also with horizontal gridding matching RO climatologies prepared in parallel in a separate project. The retrieved IASI temperature and humidity profiles and IASI sea surface temperature (SST) are validated against analysis fields from ECMWF.

Temperature profiles are obtained from observations in the absorption bands of carbon dioxide (CO_2), which is a relatively abundant trace gas of known and uniform distribution. Other atmospheric constituents absorbing in the thermal IR are H_2O (water vapor and temperature sounding), O_3 (ozone profiling), N_2O , CH_4 , and CO (trace gas column amounts). The atmospheric window regions, where attenuation is minimal, are used to obtain surface and cloud properties. With the opportunity of a very high spectral resolution at several wavelengths, the possibility of observing different height layers can be established by taking into account that radiances measured near the center of an absorption band arise from the upper atmospheric layers, while measurements at the wings of a band will sense deeper into the atmosphere.

One of the primary objectives of the IASI instrument, according to the IASI science plan (*Camy-Peyret and Eyre* (1998)), is the improvement of the vertical resolution of temperature and water vapor profiles to about 1 km in the middle and lower troposphere as well as improving the retrieval accuracy to within 1 K in temperature and $\sim 10\%$ in humidity. A main scientific motivation of this is based on the key role of water vapor in the upper troposphere and its effects on the global climate since only small changes in humidity and its trends have serious implications on the amount of thermal energy escaping to space (*Schmetz et al.* (1995); *Spencer and Braswell* (1997)). Additionally, this level of performance will greatly assist numerical weather prediction (NWP) in delivering accurate and frequent temperature and humidity profiles for operational and research needs and it will supply more accurate quantifications of climate variability, particularly contributing to our knowledge of the climate of the upper troposphere.

The main goal of this report is the validation of atmospheric profiles (temperature, humidity, ozone) and SST, retrieved from real IASI data with the developed processing system, against ECMWF analysis fields. Additionally it describes the preparation of a climatology processing system, which uses the heritage of radio occultation projects but is extended regarding the higher data density of the IASI instrument compared to radio occultation measurements. Section 2 describes the validation of atmospheric profiles (temperature, humidity, and ozone) against high resolution ECMWF analysis fields. In section 3 the preparation of the climate processing is described and its functioning demonstrated. Finally, section 4 presents a summary and the main conclusions of the report and an outlook to the next steps of work.

2 Validation of Atmospheric Profiles and SST from MetOp IASI

This section contains the "IASI Validation Report" part of the two main sections, 2 and 3, of this report.

2.1 Validation Setup and Validation Datasets

2.1.1 Advanced Infrared Sounding with the MetOp IASI Sensor

Earth observation via space-based remote sensing has a history dating back to the TIROS (Television Infrared Observation Satellite) Program of the early 1960's starting with the launch of TIROS-1 on April 1, 1960, which had an operational period of only 78 days. Since that time satellite-based meteorology was improved by, e. g., the first determinations of atmospheric humidity and temperature profiles carried out by the NIMBUS satellite series in the early 1970's which also started to perform ozone measurements. In the last two decades, further improvements have been made on the horizontal sampling and accuracy of retrievals particularly with instruments such as the High Resolution Infrared Sounder (HIRS), as well as on the vertical resolution of the data by the Atmospheric Infrared Sounder (AIRS) on-board of the AQUA Satellite. Today's global system of meteorological satellite observations include geosynchronous spacecrafts flying at an altitude of about 36000 km and polar-orbiting satellites in low earth orbits of about 800 km.

The Infrared Atmospheric Sounding Interferometer (IASI), which will be part of the core payload of the METOP series of polar orbiting operational meteorological satellites currently prepared for EUMETSAT (first satellite to be launched in 2005), will provide a further significant improvement of vertical resolution of temperature and humidity profiles compared to existing operational satellites via a very high spectral resolution. Furthermore it will deliver ozone profiles and surface skin temperature as well as cloud parameters and column amounts of nitrous oxide (N_2O), methane (CH_4), and carbon monoxide (CO).

IASI is a Michelson type Fourier transform interferometer, which samples a part of the infrared (IR) spectrum contiguously from 645 cm^{-1} to 2760 cm^{-1} ($15.5\text{ }\mu\text{m}$ – $3.6\text{ }\mu\text{m}$) with an unapodized spectral resolution of about 0.5 cm^{-1} . The acquisition of information about the surface and the atmosphere is based on detection, recording, and analysis of electromagnetic (EM) radiation emitted by the earth mainly in the infrared range of the EM spectrum. The characteristics of the modification of radiation when passing through the atmosphere depends on the amount and properties of the atmospheric constituents. Therefore the information about the state of the atmosphere stored in the detected radiation may be retrieved from the measured spectrum.

Temperature profiles are obtained from observations in the absorption bands of carbon dioxide (CO_2), which is a relatively abundant trace gas of known and uniform distribution. Other atmospheric constituents absorbing in the thermal IR are H_2O (water vapor and temperature sounding), ozone (O_3 – ozone profiling), N_2O , CH_4 , and CO (trace gas column amounts). The atmospheric window regions, where attenuation is minimal, are used to obtain surface and cloud properties. With the opportunity of a very high spectral resolution at several wavelengths, the possibility of observing different layers can be established by taking into account that radiances measured in the center of an absorption band arise from the upper atmospheric layers, while measurements at the wings of a band will sense deeper into the atmosphere.

Figure 1 shows as an example an real IASI measurement at 31.16°N and 155.43°E . Overplotted are the selected channels which are used in the channel selection comparison study of section 2.3.1.

2.1.2 IASI Test Orbit Data and ECMWF Reference Data

The retrievals performance assessments discussed in this report were based on real IASI data from a test orbit distributed by EUMETSAT. The measurements started on April 2, 2007 at 23:20 and ended on April 3, 2007 at 0:23.

The number of independent earth scans for this orbit is 91800. This number is then reduced by taking only the cloud free pixels (the cloud flags are a product of the IASI Level 2 processor and are also obtained by EUMETSAT) as well as those measurements occurring over land. Additionally, only the five smallest scan angles in each direction, i. e., 40 measurements per scan line were taken into account. A further reduction of the measurements had to be accepted by rejecting those channels which are lying beyond 70° north or south to account for possible occurrence of sea-ice ground-pixels. This final reduction was performed due to the fact that for the outer scan angles bending effects would have been taken into account. After this about 500 measurements remained. Due to the fact that we had only one orbit of data there was no possibility to perform an independent bias correction. Hence, an additional quality control step was implemented which selects out all profiles where the difference in brightness temperature between the forward modeled first guess and the measurements are larger than 10°K.

Figure 2 shows the ground track and swath width of the full orbit – the orbit starts with its descending node ranging from the Arctic regions north of the Kamtschatka peninsula over the Western Parts of the Pacific Ocean and Australia to Antarctica and then with its ascending node via the Atlantic Ocean and America back to the Arctic Regions. The red line of dots in the middle indicates the nadir points of the MetOp satellite for every scan line, the dots in dark violet represent the borders of the scanning region of the IASI instrument. The green crosses are the points of the measurements selected for the processing, the blue crosses are those points finally retrieved.

For the initialization of and as *a priori* data to the retrieval we used the 24-hour ECMWF forecast field (T5111L91 resolution, e. g., *ECMWF* (2004)) for April 3, 2007, 00 UTC. The individual values along the profiles were obtained by interpolating the values of the forecast field to the locations according the RTIASI pressure level grid and the ground points of the measurements, respectively. The version of RTIASI used in the current stage of the report is RTIASI 1.0 (*Matricardi and Saunders* (1999)).

Temperature and Ozone were retrieved over the whole RTIASI pressure level range. Additionally, the surface air temperature (2 m temperature) and the surface skin temperature were added to the retrieval process to obtain an excellent surface retrieval. In the case of humidity only the lowest 28 levels (up to ~100 hPa) were introduced in the joint retrieval since the stratosphere (at <100 hPa) is a very dry region and the humidity information which can be gained there by the IASI instrument is negligible.

As reference field, for performing the error analysis, an ECMWF analysis field (T511L91 resolution) for April 3, 2007, 00 UTC was used.

2.1.3 Validation Methodology

In the enhancement report of the MULTICLIM project the retrieval algorithm, the covariance matrix setup, the description of the forward model, and the channel selection were explained in detail. Figure 1 once more gave an overview of the selected channels – but now with a true profile as reference in the background.

In addition, the validation in the following sections is based on error statistics of temperature, humidity and ozone profiles. For each corresponding pair of profiles (\mathbf{x}_{ret} , being the retrieved profile and \mathbf{x}_{ref} , being an ECMWF profile) a difference profile $\Delta\mathbf{x}$ was derived ($\Delta\mathbf{x} = (\Delta x_1, \Delta x_2, \dots, \Delta x_i, \dots, \Delta x_n)^T$, with $i = 1, \dots, n$ denoting the height levels and T the matrix

transpose):

$$\Delta \mathbf{x} = (\mathbf{x}_{ret} - \mathbf{x}_{ref}) \quad (1)$$

The calculation of the mean of the difference profiles lead to the bias profile \mathbf{b} ,

$$\mathbf{b} = \left[\frac{1}{n} \sum_{k=1}^N \Delta \mathbf{x}_k \right] \quad (2)$$

with N being the number of profiles in the ensemble. Next, the bias was subtracted from each profile giving bias-free profiles $\Delta \mathbf{x}^{biasfree}$,

$$\Delta \mathbf{x}^{biasfree} = \Delta \mathbf{x} - \mathbf{b}. \quad (3)$$

From these bias-free profiles we computed the error covariance matrix \mathbf{S} ,

$$\mathbf{S} = \left[\frac{1}{n-1} \sum_{k=1}^N (\Delta \mathbf{x}^{biasfree}) (\Delta \mathbf{x}^{biasfree})^T \right], \quad (4)$$

with its diagonal elements representing the variances S_{ii} at height level i and with its non-diagonal elements representing the covariances S_{ij} between height level i and j . The square root of its diagonal gives the standard deviation profile \mathbf{s} with:

$$s_i = \sqrt{S_{ii}}, \quad (5)$$

The root mean square error profiles \mathbf{rms} writes:

$$rms_i = \sqrt{b_i^2 + s_i^2}. \quad (6)$$

Throughout this report temperature differences are given in terms of absolute quantities and humidity and ozone differences in terms of relative quantities. The relative quantities are derived by dividing the absolute quantities by the mean of the reference profiles \mathbf{x}_{ref} at each altitude.

2.2 Temperature, Humidity, Ozone, and SST Validation

The aim of this section is to proof that the algorithm is working with real data on the one hand and on the other hand to show the performance of our algorithm with real IASI data.

2.2.1 Validating Temperature, Humidity, and Ozone Profile Retrievals

Figure 3 shows the results of the retrieval process for temperature (first row), humidity (second row) and ozone (third row), respectively, for the estimation results for the case when using ~ 300 channel set. The final number of retrieved profiles for this set was 95. With the ECMWF profiles as reference profiles, the panels show bias (solid black line), standard deviation (solid gray line), rms error (dashed black line), standard error (square-root of diagonal elements) specified in the *a priori* error covariance matrices (dashed-dotted black line), and, in panels b, d, and f, standard error (square-root of diagonal elements) as defined in the retrieval error covariance matrices (dashed-dotted gray line), respectively. Panels a, c, and e directly exhibit the errors of the *a priori* profiles compared to the reference profiles showing that these have been conservatively set for temperature and humidity (outer-bound envelope to the error estimates for the present forecast-minus-analysis data used).

On a first view of the temperature results we can see that there are nearly no changes in the standard deviation but a shift of the mean difference which clearly shows that the IASI

data has an impact on the ECMWF background data. It can be seen that there are problems in resolving the tropopause. Figure 4 provides a more closer examination of the temperature results: We can see the features obtained by retrieving the IASI data on both latitude bands. In both regions the systematic deviation of the retrieval compared to the ECMWF analysis in the mid and lower troposphere is about 0.5°K . In the stratospheric parts of the atmosphere the information contained in the IASI data is able to reduce the bias contained in the first guess data. The reason that no data from 60° – 90° is shown here is, that there was made an additional cut off of the data to avoid contamination of measurements with sea ice ground points.

Comparing the results of the retrieved humidity (panel d of Figure 3) with the first guess (panel c), mostly the same can be said as in the case of the estimation of temperature. However, both Figures, Figure 3 and Figure 5 we can see the promising results in the upper troposphere (>500 hPa) leading to the result of an quite useful climate monitoring upper tropospheric humidity (UTH) product.

In the case of the retrieved ozone profiles (panel f) of Figure 3 as well as Figure 6 we obtain a shift of the mean profile compared to the first guess and analysis profile of ECMWF which is in evidence. In the stratosphere the bias compared to ECMWF is positive whereas it is negative in the troposphere. This could imply that the ozone in the ECMWF model is incorrect.

2.2.2 Validating Sea Surface Temperature (SST) Retrievals

Figure 7 illustrates the retrieval performance of the SST. In contrast to the SST results shown in the enhancement report (*Schwaerz et al. (2007)*) where the retrieval exhibits better results for the rms error than the theoretical estimate in the retrieval error covariance matrix (S_{ret}) proposes we of course have a larger deviation of the retrieval results with real data. The more detailed results given in Figure 8 do not exhibit larger deviations for on or the other case.

However an interesting feature is that they have opposite biases, especially, this is interesting in the case of the mid latitudes (30° – 60° , panel c and d) where the bias of the forecast is positive and that of the retrieved SST is negative. The reason therefore could lie on the one hand in the very smooth structure of ECMWF SST's as well as in an upcoming representativeness error but on the other hand of course an insufficient radiative transfer could have led to an insufficient retrieval.

2.3 Channel Selection Methods and Single-Parameter Retrieval Assessment

2.3.1 Comparison of Information-Content and Maximum-Sensitivity Channel Selection

In this section the retrieval performance based on the two different channel selection algorithms described in the enhancement Report (*Schwaerz et al. (2007)*) (IC and MS approach) is comparatively assessed for two sets of numbers of selected channels. For all four cases we used the same dataset as described in section 2.1.2 above. The assessment is to reveal which channel selection approach is to be potentially preferred for the planned climate monitoring setup and whether a channel reduction to as low as ~ 300 channels is possible without relevant performance degradation of the joint algorithm retrieval products.

The two different sets of numbers of selected channels were chosen with the target to get approximately 3.5% and 10% of the full number of IASI channels (8461) which resulted in an averaged number of selected channels per profile of ~ 300 (300) channels for the smaller dataset ($\sim 3.5\%$) and ~ 900 (887) channels for the larger dataset ($\sim 10.6\%$). On a closer examination this can be split up into the different atmospheric parameters (and SST) the channels are selected for. To this end, more precisely, the averaged numbers of selected channels per profile were 89/324 channels for temperature, 87/336 for humidity, 64/167 for ozone and 60/60 for SST,

respectively. We see that the number of selected channels for the different atmospheric species do not follow the rough multiplication factors between total sets ($3.5\% \times 3 \approx 10\%$). The reason is that the IASI spectral interval has only two small bands for the surface (SST) and the ozone channels (c. f. Figure 1) which means that the number of channels with reasonable information for these parameters is limited. Thus we have filled up the remaining amount by temperature and humidity channels.

Number of Profiles		
channel set	IC	MS
300	95	78
887	21	21

Table 2: Comparison of the finally retrieved number of Profiles for the four different channel selection cases.

Figure 9 (for temperature) and Figure 10 (for humidity) illustrate the inter-comparison of the results for the different cases. Ozone and SST inter-comparison are not explicitly shown. As they do not add further aspects to the discussion and conclusions we draw from assessing temperature and humidity. An overall view on Figures 9a-d and 10a-d already provides clear evidence that the performance differences are fairly small amongst all 6 cases although the numerical efficiency is of course drastically better for the case of selecting about 3.5% of the channels only. It has to be mentioned that due to the additional quality control step which was implemented since no independent bias correction was available (rejection of all profiles where the difference in brightness temperature between the forward modeled first guess and the measurements are larger than 10 K) the number of processed measurements is different in all four cases. Table 2 summarizes the number of profiles processed for the different cases. It can be seen that in the case of the small number of selected channels, for both channel selection methods (with IC and MS approach) almost the same number of measurements were processed whereas in the case of about 800 selected channels only about 25% were not rejected.

On a closer examination of the temperature results (Figure 9) we serve that the MS approach results in a slightly higher bias as well as standard deviation (and rms, respectively) than the IC method in the troposphere. For both methods we obtain a clear problem in resolving the tropopause whereas in the stratosphere the standard deviation is smaller for the IC approach than for the MS approach.

A comparison of the two different numbers of selected channels (panel a and b versus panel c and d of Figure 9 left column IC; right column MS) exhibits slightly worse results for the standard deviation in the case of ~ 800 channels but a better resolution of the tropopause for the same sets. The reason therefore is not clear, yet, and has to be further investigated. Possible explanations are a better set of channels for the tropopause region or that the measurement which causes the large bias structure in the tropopause region was selected out by the maximum brightness difference criteria in the case of ~ 800 channels.

Inspecting the humidity results more closely (Figure 10), we find that these show analogous behavior to the temperature results, i. e., no explicit gain in retrieval performance but rather increasing numerical residual error effects for an increasing number of channels. On an adequate and sufficient number of channels for the joint algorithm we thus conclude that ~ 300 channels is an excellent and numerically efficient choice; even lower numbers start to imply performance degradation.

Regarding the preferable channel selection approach, we find that the MS approach has fairly the same but no better efficiency as the IC approach and closely similar but no better performance. Tentatively the IC approach performs slightly better, presumably due to the more

even distribution of the selected channels (c. f. *Schwaerz et al. (2007)*), and the IC approach has theoretically a better foundation, so that we chose this one as the baseline for future large-scale application of the algorithm.

2.3.2 Comparison of Joint Multi-Parameter Retrieval to Single-Parameter Retrieval

We evaluated for the joint retrieval algorithm described in the enhancement report (c. f. *Schwaerz et al. (2007)*) how it improves over more specific single-parameter retrieval setups. This provides valuable further tests on the robustness and quality of the joint algorithm, but also allows to assess to what degree more simplified (and thus even faster) setups may be applicable. As input set for all cases discussed here, we used climatology-based channel selection by the IC approach for selecting ~ 300 channels in total and again the full orbit arc dataset as done in the simulation study in the enhancement report of the current project.

Figure 11 illustrates the results comparing joint retrieval to single-parameter retrieval where single-parameter retrieval means that one parameter (e. g., temperature) is retrieved while the others (e. g., humidity, ozone, SST) are kept fixed at their *a priori* values. We do not separately discuss ozone here since its retrieval is rather independent of the other parameters (*Schwaerz et al. (2007)*), so that the results of joint and single-parameter retrieval are essentially the same.

Regarding temperature (Figure 11a, b) we can identify two regions where we obtain a growth in standard deviation (and rms), which were also noted in the enhancement report (c. f. *Schwaerz et al. (2007)*). The first is the boundary layer where on the one hand a detailed analysis of the results of the simulation study (c. f. *Schwaerz et al. (2007)*) yielded a warm bias in the tropical and mid-latitude region originating from a warmer surface than the overlying atmosphere and on the other hand a cold bias occurring over Antarctica where the surface is generally colder than the atmosphere. This problem is mainly resulting from the absence of a simultaneous SST retrieval based on the inclusion of surface channels, as done in the joint retrieval. The second region where the joint retrieval algorithm is clearly superior is the troposphere (below ~ 300 hPa) where the absence of the simultaneously retrieved humidity results in rms temperature error increases of about 2/3. For stratospheric retrievals the differences are small.

Regarding humidity (11c,d) the essential difference is evidently that the joint retrieval can achieve a clearly better rms error than the humidity-only retrieval.

This is since the joint retrieval accounts for the temperature-humidity coupling, while the humidity-only retrieval cannot do so. Still the latter works fairly well here thanks to the high quality *a priori* temperature profiles from the ECMWF 24h forecast; in the case of a worse temperature input, the humidity-only retrieval may also incur biases up to $\sim 10\%$.

Regarding SST (Figure 11e, f), the joint temperature, humidity, ozone, and SST retrieval shows a drastically improved performance with an rms error which is better by almost a factor of 2.

Closer examination of the error analysis results in the enhancement report (c. f. *Schwaerz et al. (2007)*) showed that the main reason for this large difference lay in the tropics, more exactly, in regions with warm sea surface temperature. The main physical reason behind is the significant water vapor continuum absorption over warm tropical oceans even in the "atmospheric window" channels (e. g., *Liou (2002)*) which strongly degrades the SST-only retrieval.

In summary it is clear that the joint temperature, humidity, ozone, and SST retrieval algorithm exhibits a significantly improved performance over the single-parameter retrieval setups, and is thus our obvious baseline for future large-scale climate monitoring application. While this is itself neither new nor surprising the understandable and robust way in how our newly developed IASI processing system behaves both in joint and single-parameter mode provides us with substantial confidence in its utility for future applications.

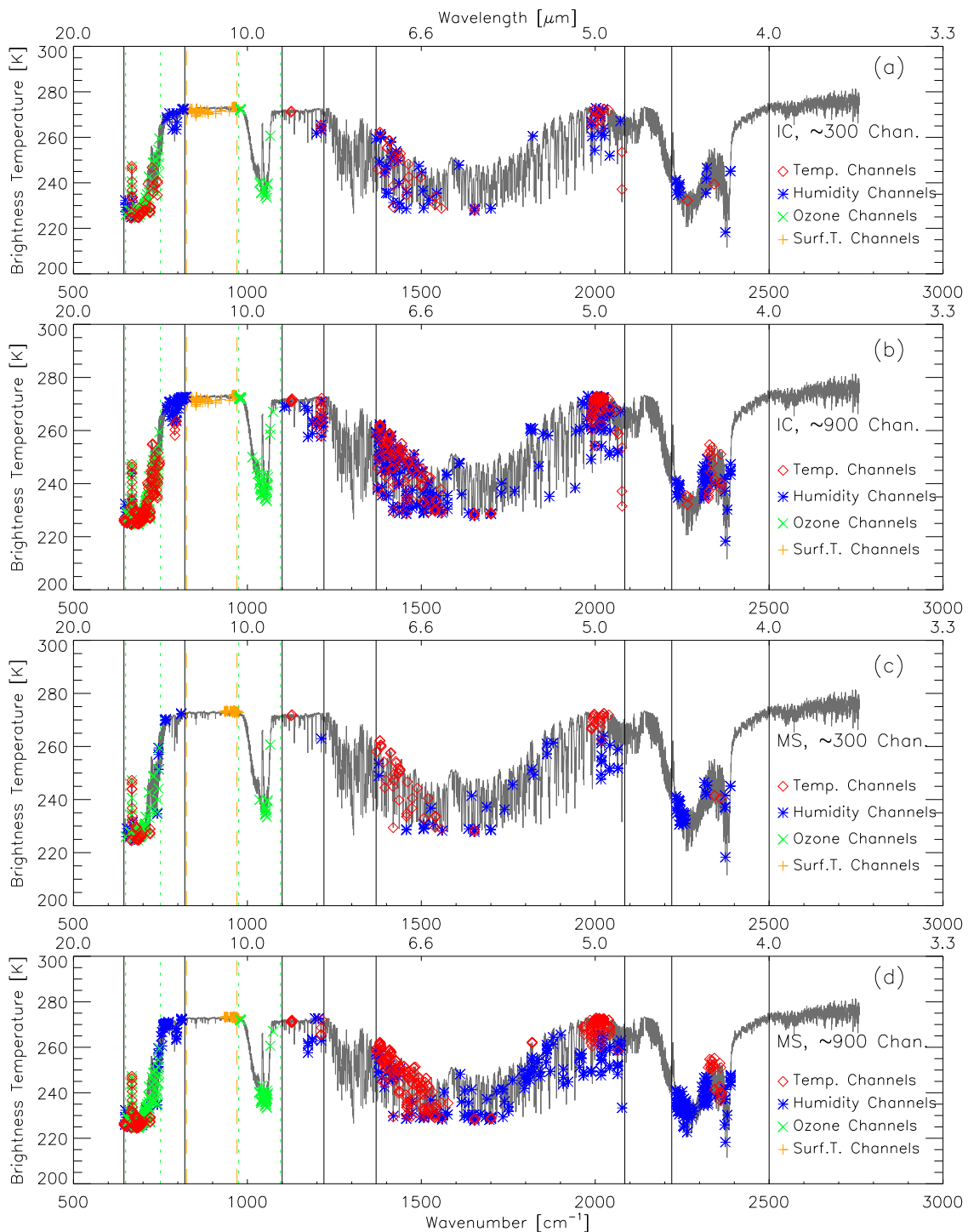


Figure 1: Selected channels for temperature, humidity, and ozone profiles as well as for SST over-plotted on the brightness temperature spectrum of an observed profile at 31.15°N and 155.42°E. The diamonds indicate the temperature channels, the asterisks the humidity channels, the crosses the ozone channels and the plus signs the SST channels. Panels a and b depict the selection based on the IC approach whereas panels c and d the one for the MS approach. The total number of selected channels for panels a and c (adding the channels for all constituents) was 310, whereas the total number for panels b and d was 909. The vertical lines delimit the regions within which the channels for the different atmospheric species were selected. Solid lines: temperature and humidity, dashed lines: SST, dotted lines: ozone.

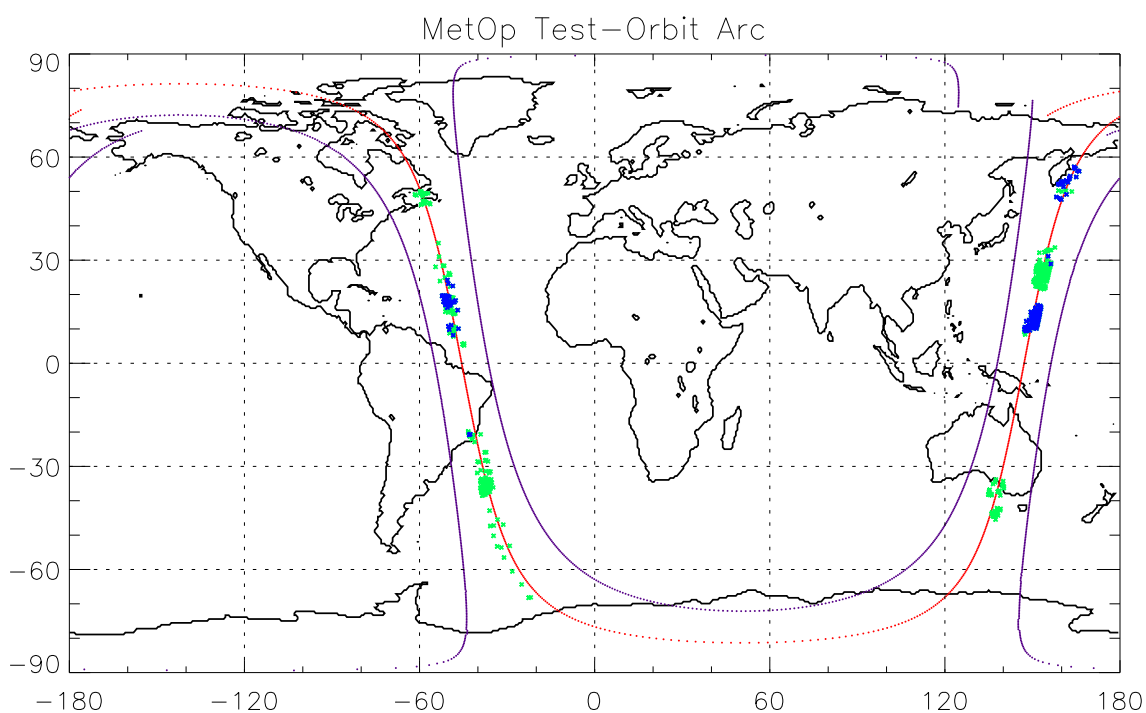


Figure 2: Ground track and lateral width of the IASI swath simulated for one MetOp orbit, depicted on a world map. The line of dots in the middle indicates the nadir points of the MetOp satellite for about every 8-th second (IASI swath sampling time). The green crosses are the points of the measurements selected for the processing, the blue crosses are those points finally retrieved.

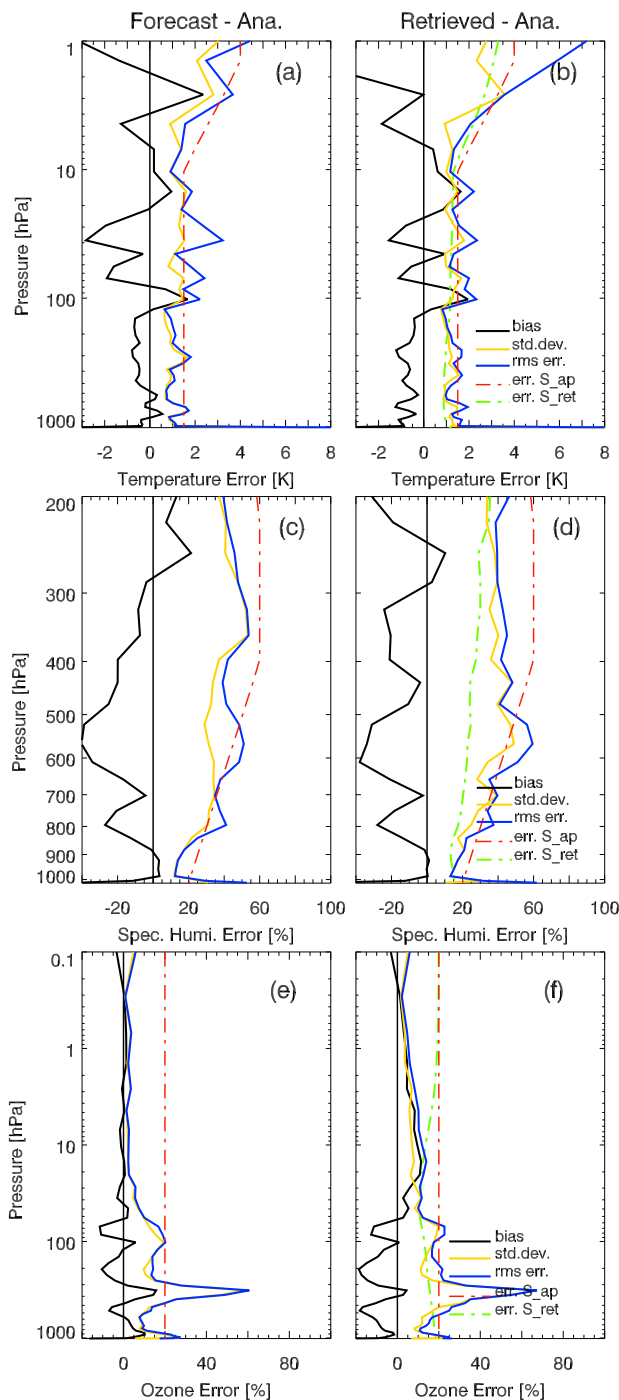


Figure 3: Results of the joint retrieval algorithm for temperature (left column), humidity (middle column) and ozone (right column). Bias (solid black line), standard deviation (solid gray line), rms error (dashed black line), standard error (square-root of diagonal elements) specified in the *a priori* error covariance matrices (dashed-dotted black line), and, in panels d – i, standard error (square-root of diagonal elements) as defined in the retrieval error covariance matrices (dashed-dotted gray line). Panels a – c directly exhibit the errors of the *a priori* profiles compared to the reference profiles.

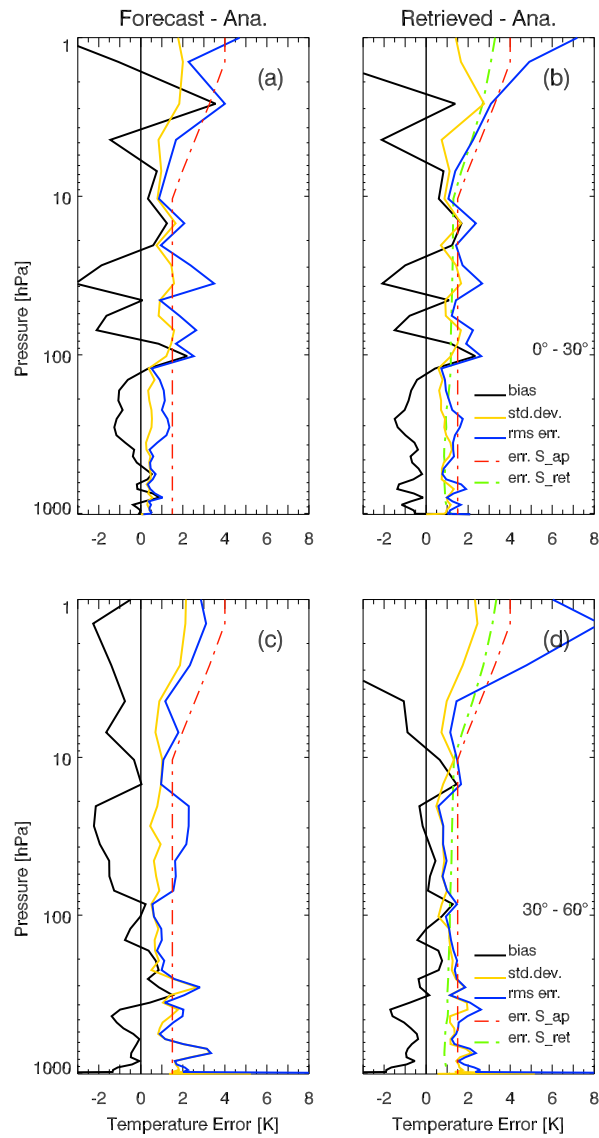


Figure 4: Temperature results separated into two latitude bands (0°–30° and 30°–60°). Explanation see Figure 3.

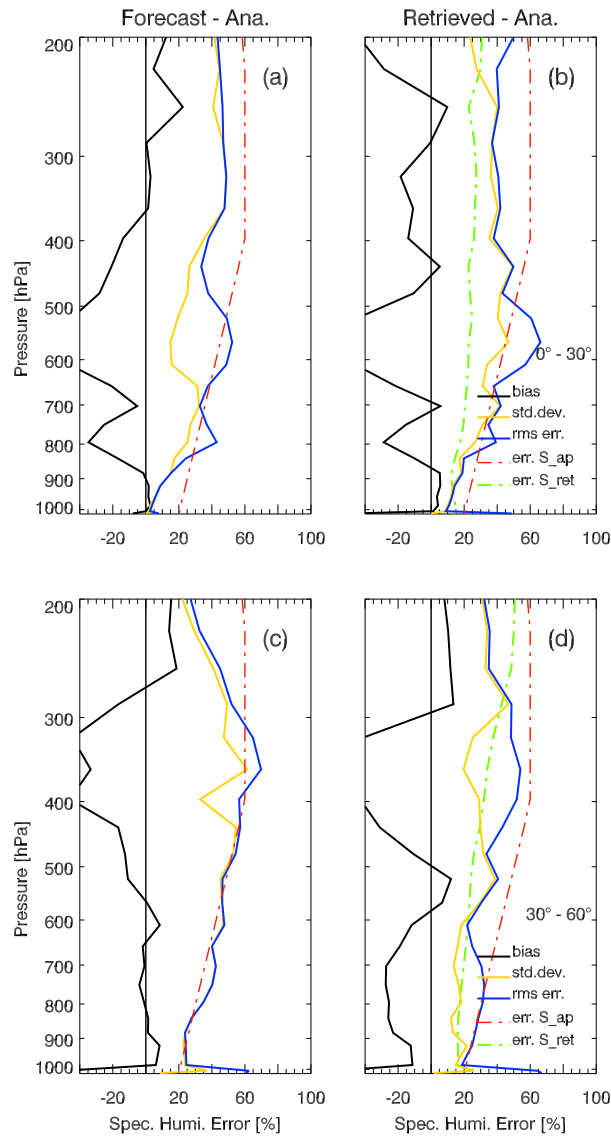


Figure 5: Humidity results separated into two latitude bands (0° – 30° and 30° – 60°). Explanation see Figure 3.

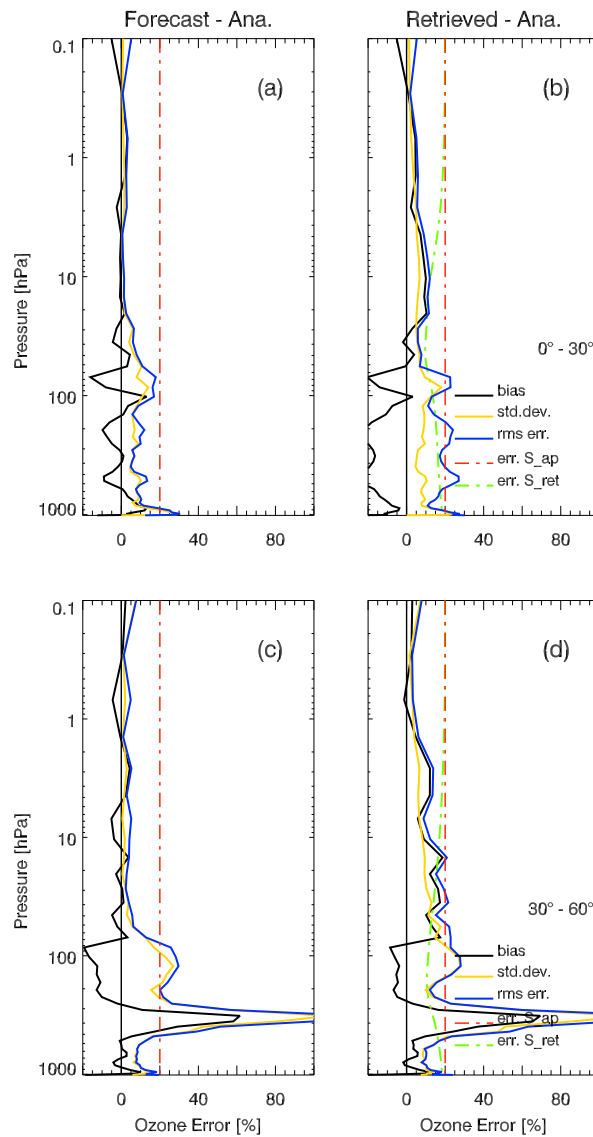


Figure 6: Ozone results separated into two latitude bands (0° – 30° and 30° – 60°). Explanation see Figure 3

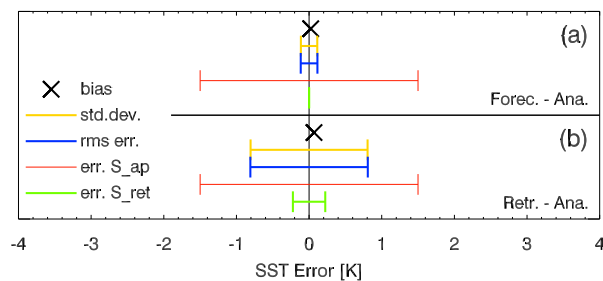


Figure 7: Results of the joint retrieval algorithm for SST. Bias (black cross), standard deviation (dark-gray error bars), rms error (black), standard error (square-root of diagonal element) specified in the *a priori* error covariance matrices (light black), and, standard error (square-root of diagonal element) as defined in the retrieval error covariance matrices (light gray).

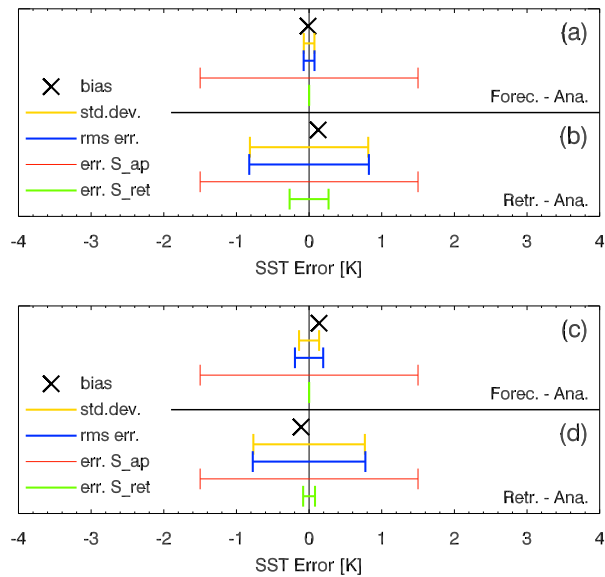


Figure 8: SST results separated into two latitude bands (0°–30° – panel a) and b), 30°–60° – panel c) and d)). Explanation see Figure 7.

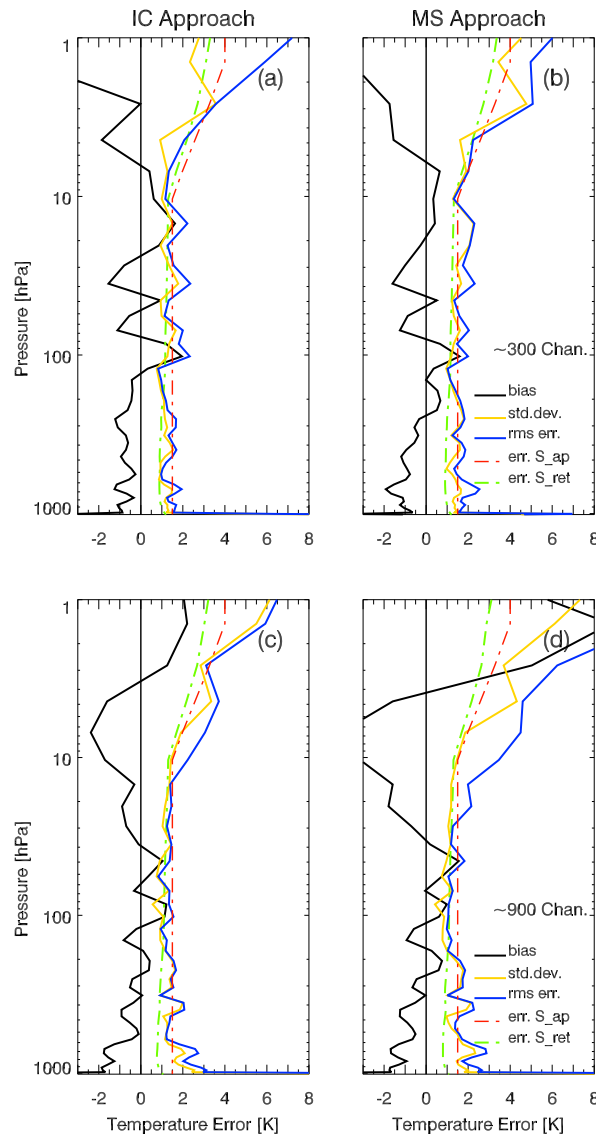


Figure 9: Temperature results of the joint retrieval algorithm for six different retrieval cases (3 channel numbers, each for IC and MS approach). Bias (solid black line), standard deviation (solid gray line), rms error (dashed black line), standard error (square-root of diagonal elements) specified in the *a priori* error covariance matrices (dashed-dotted black line), and the standard error (square-root of diagonal elements) as obtained in the retrieval error covariance matrices (dashed-dotted gray line).

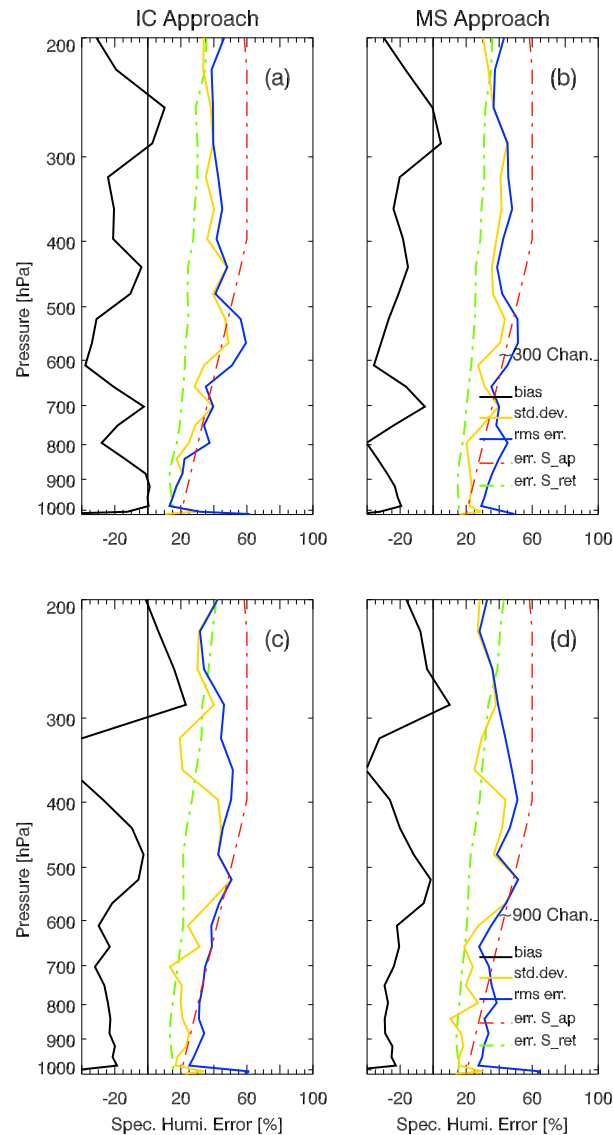


Figure 10: Humidity results of the joint retrieval algorithm for six different retrieval cases (3 channel numbers, each for IC and MS approach). Bias (solid black line), standard deviation (solid gray line), rms error (dashed black line), standard error (square-root of diagonal elements) specified in the *a priori* error covariance matrices (dashed-dotted black line), and the standard error (square-root of diagonal elements) as obtained in the retrieval error covariance matrices (dashed-dotted gray line).

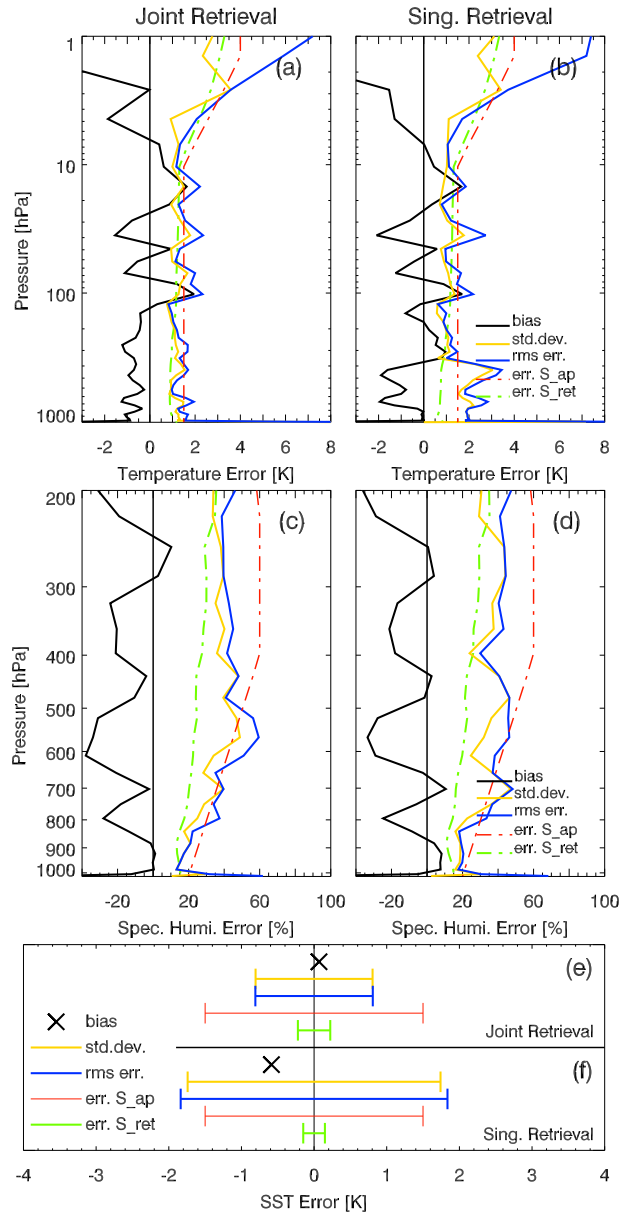


Figure 11: Comparison of the results for multi-parameter retrieval and single-parameter retrievals for temperature (upper panels), humidity (middle panels), and SST (lower panels), respectively. Bias (solid black line; SST: black cross), standard deviation (solid gray line; SST: dark-gray error bars), rms error (dashed black line; SST: solid black), standard error (square-root of diagonal elements) specified in the *a priori* error covariance matrices (dashed-dotted black line; SST: solid light black), and the standard error (square-root of diagonal elements) as obtained in the retrieval error covariance matrices (dashed-dotted gray line; SST: solid light gray).

3 Preparation of Climatology Processing

3.1 Grid Definitions and the Climatology Processing System (CLIPS)

In this section, subsection 3.1.1 describes the geographic regions and further definitions that have been used for demonstrating the prepared climatology processing for IASI and subsection 3.1.2 introduces the WegCenter’s climatology processing system CLIPS that has been prepared to ingest also IASI retrieved profiles in addition to radio occultation profiles (cf. *Pirscher et al.* (2007)).

3.1.1 Climatological Averaging Grid Definition, Datasets, and Example Season

We have used three representative grid definitions from high to very coarse in order to demonstrate the prepared climatology processing: a high resolution, set to $5^\circ \times 5^\circ$ (latitude x longitude), as would be typically available for IASI data (but is not for radio occultation data), a coarser resolution, set to $5^\circ \times 60^\circ$ (latitude x longitude), typical for radio occultation (with multiple satellites), and a very coarse resolution, set to 10° latitude resolution of zonal bands, typical for more global-scale resolution applications (latitude-resolved global climate monitoring).

Given that for IASI data we do not yet have available datasets of climatological lengths (e.g., months or seasons of climate quality-processed data) we used "IASI proxy" profiles extracted from ECMWF analyses at a resolution of $2.5^\circ \times 2.5^\circ$ over all individual six-hourly analysis fields of a full climate period (such as month or season). As an example climate season for demonstration, we selected a representative season (September-October-November 2006, SON 2006).

For providing real data reference climatology processing for the coarser resolution data as well as for the zonal-band resolution data we also included COSMIC and CHAMP radio occultation data at these resolutions and compared them to the "IASI proxy" climatologies sampled from ECMWF analyses.

Figure 12 illustrates the selection of the different resolution grids as well as the geographic distribution of the retrieved profiles of the real datasets (COSMIC and CHAMP) over the demonstration time period (SON 2006).

It is well visible that $5^\circ \times 5^\circ$ is potentially a very attractive climate monitoring potential of IASI, though also with this sensor the real sampling will depend on the distribution of clear and cloudy scenes since persistent cloud cover (e.g., over weeks) reduces the number of climatologically useful IASI profiles in a region. Also the COSMIC data (six satellite radio occultation constellation; cf., e.g., *Pirscher et al.* (2007)) give, over a season, a quite dense resolution, and, being radio occultation data, have high vertical resolution and sample also cloudy scenes (all-weather capability). However, IASI is strongly superior in horizontal resolution, so that despite of cloud sensitivity its horizontal climatologies will be denser.

3.1.2 Overview of the Climatology Processing System CLIPS

The CLIPS system was developed at Wegener Center for processing retrieved profiles from radio occultation data into climatologies of different resolutions, starting with $2.5^\circ \times 2.5^\circ$, and for different variables (such as temperature and humidity). As IASI retrieved profiles, if available in a joint format with radio occultation data exhibit, from the point of view of binning and averaging them into climatologies, no structural differences, we could without major problems also adjust the CLIPS for processing IASI profiles in addition to radio occultation profiles.

Figure 13 shows an overview of the CLIPS system. It starts with the ingestion of retrieved profiles, relevant here those from the IASI processing system ("IASI PS"; upper left corner of Figure 13), and then processes these into user-defined climatologies. Testing this system with

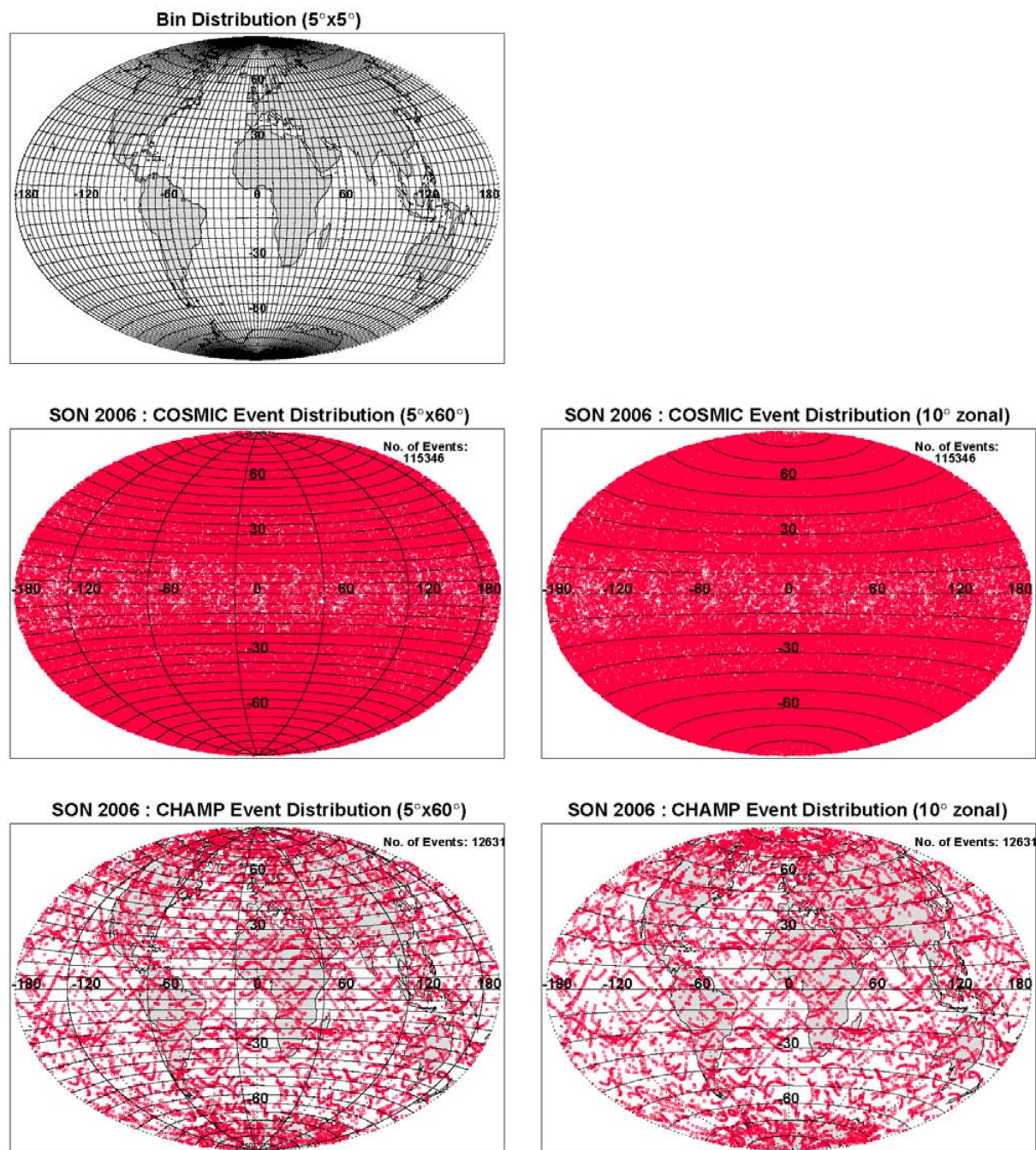


Figure 12: Overview of example geographical grid resolutions and example data distributions. $5^\circ \times 5^\circ$ high resolution as typical for future IASI data (top left), $5^\circ \times 60^\circ$ coarser resolution with COSMIC SON2006 data as example (middle left), $5^\circ \times 60^\circ$ coarser resolution with CHAMP SON2006 data as example (bottom left), 10° zonal-band resolution with COSMIC SON2006 data as example (middle right), and 10° zonal-band resolution with CHAMP SON2006 data as example (bottom right) are shown.

the "IASI proxy" data, which we sampled from ECMWF analyses, renders it prepared also for processing real IASI retrieved profiles ingested into the same CLIPS input format.

We do not enter here into a detailed description of the CLIPS components and structure as visible in Figure 13, since CLIPS has been recently described in detail by *Pirscher et al. (2007)*, where the interested reader is referred to for more information.

3.2 High-Resolution and Zonal-Band Climatology Processing Demonstration

In this section we show climatology processing results that well demonstrate the functioning of the CLIPS system now also prepared for IASI-based climatologies. We show that from different perspectives, "slices" and "maps" through the data, to give a decent view of the value of different resolutions. Subsection 3.2.1 shows examples of Latitude-Altitude slices, subsection 3.2.2 of Latitude-Longitude maps, and 3.2.3 of zonal-band resolution slices and maps, respectively. We show all examples for temperature, more precisely dry temperature, a variable inherited from radio occultation, which does, however, not appreciably differ from the "normal" physical temperature at altitudes of 10 km and beyond which are the focus here (see *Foelsche et al. (2007)* for a detailed definition and explanation of dry temperature).

3.2.1 Demonstration of Latitude-Altitude Climatological Resolution

Latitude-Altitude slices of climatologic temperature fields give a good impression on vertical structures in the atmospheric temperature field and on its equator-to-pole variability.

Figure 14 shows such slices at two different meridians, a European-African and (North-)American one, for the high resolution "IASI proxy" data (i.e., densely sampled from the ECMWF analysis fields as described above) but also for the coarser resolution data. This highlights the different information gain at different resolutions. The difference, at coarser resolution, of the temperature climatologies from the real COSMIC data relative to those from the densely sampled "IASI proxy" data, is shown as well. It illustrates, at a given common climatological resolution, the differences between the somewhat less densely sampled COSMIC climatologies and "IASI proxy" (ECMWF) climatologies. More technically the slices demonstrate that the prepared climatology processing works in a good manner.

3.2.2 Demonstration of Horizontal (Latitude-Longitude) Climatological Resolution

Latitude-Longitude maps of climatologic temperature fields give a good impression on the geographical variability in the atmospheric temperature field all over the globe and can be inspected at different altitudes in order to get insight into the height dependence of geographical variability of the climate.

Figure 15 shows such maps at two different altitudes, an upper tropospheric and a lower stratospheric one, for the high resolution "IASI proxy" data but also for the coarser resolution data. This highlights again, as for the latitude-altitude slices, the different information gain at different resolutions, now regarding horizontal-geographical variability. The difference, at coarser resolution, of the temperature climatologies from the real COSMIC data relative to those from the densely sampled "IASI proxy" data shows resolving-information differences as well. The maps furthermore illustrate, at a given common climatological resolution, also for this horizontal perspective the differences between the less densely sampled COSMIC climatologies and "IASI proxy" (ECMWF) climatologies. More technically the maps as well demonstrate that the prepared climatology processing works in a good manner.

3.2.3 Demonstration of Zonal-Band Climatological Resolution

Zonal-band climatologies, slices and maps, of climatologic temperature fields give a good impression on the overall more global-scale variability in the atmospheric temperature field and focus on the average behavior of equator-to-pole variability in both hemispheres.

Figure 16 shows both slices (left column) and maps (right column) of zonal-band temperature climatologies. Here, in addition to the climatology results for the "IASI proxy" (ECMWF) data

and the difference between COSMIC-derived and "IASI proxy" climatologies, respectively, also the difference of CHAMP single-satellite climatologies to the "IASI proxy" climatologies is illustrated. This is possible for the zonal-band resolution due to the truly large-area climatological bins in this case already (see also Figure 12), which can be "filled" with a reasonable number of profiles already by a single radio occultation satellite. For details of the merits and practical relevance of such zonal-band climatologies see *Foelsche et al.* (2007). Again, inspecting more technically, the results of Figure 16 demonstrate at yet another resolution scale the adequate functioning of the prepared climatology processing.

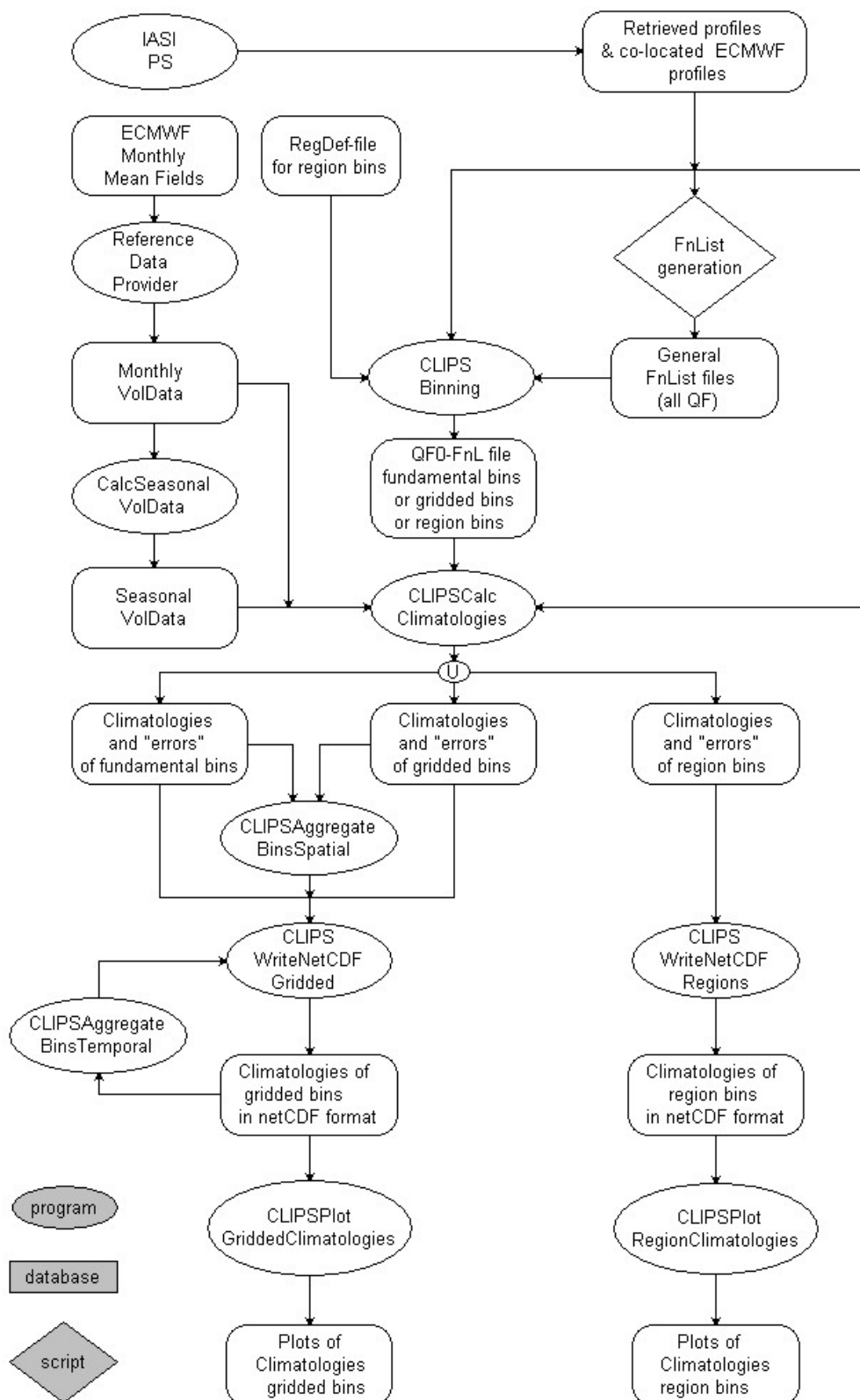


Figure 13: Overview structogram of the WegCenter's Climatology Processing System CLIPS. The CLIPS system can ingest in future retrieved IASI profiles ("IASI Processing System, IASI PS", top left) sharing the input atmospheric profiles format with other data sources like radio occultation.

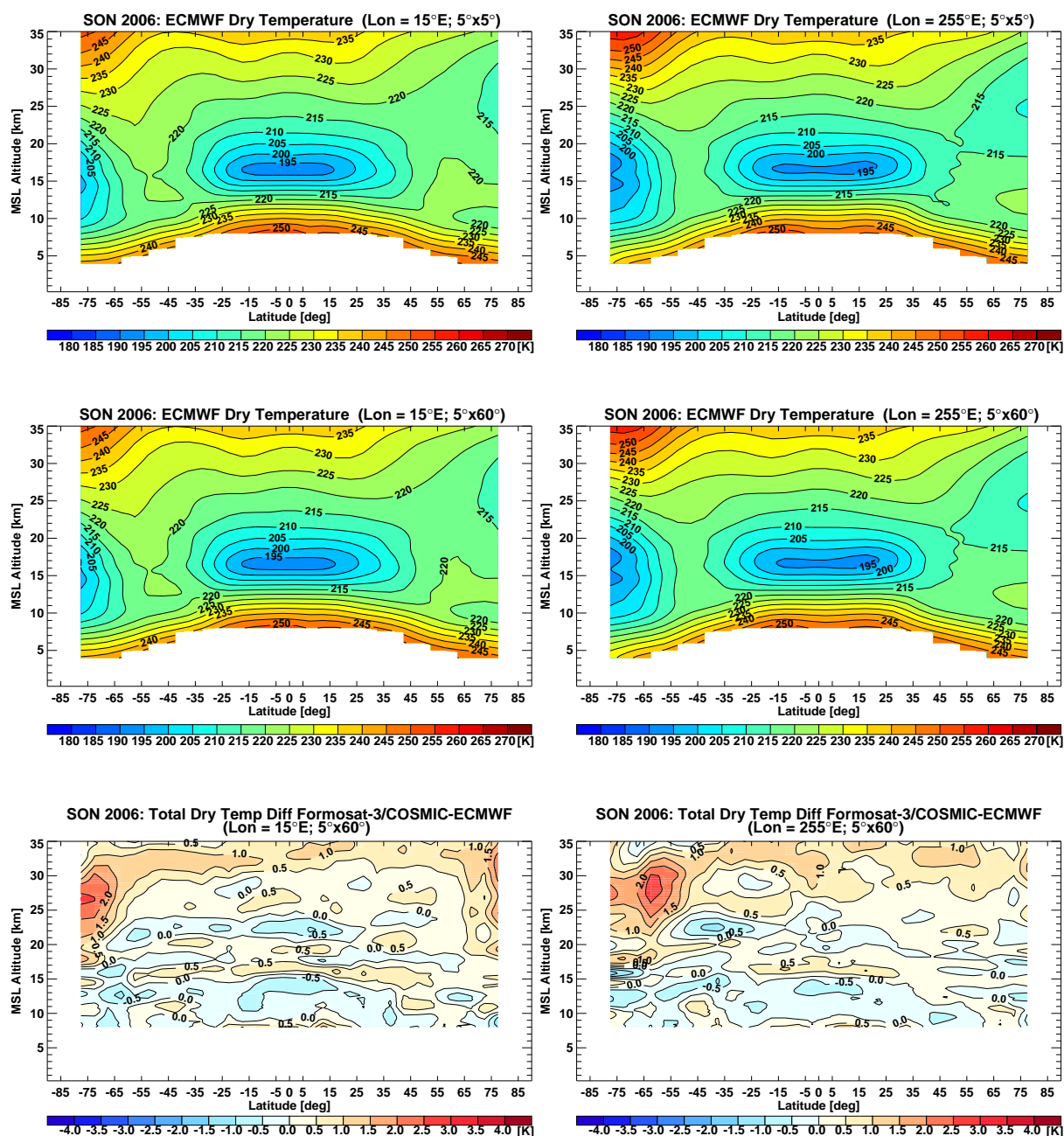


Figure 14: Latitude-altitude slices example for climate temperature monitoring, as possible in future with IASI profiles ingested into the CLIPS system, at different resolutions. Selected latitude vs. altitude example slices are shown at 15° longitude (left column; "Europe-Africa meridian") and at 255° longitude (right column; "America meridian"), respectively. What is illustrated are high resolution ECMWF climatologies as "IASI-proxy" data (top row), coarser resolution ECMWF/"IASI-proxy" climatologies (middle row), and the difference between coarser resolution COSMIC climatologies from real profiles and the corresponding coarser resolution ECMWF/"IASI-proxy" climatologies (bottom row).

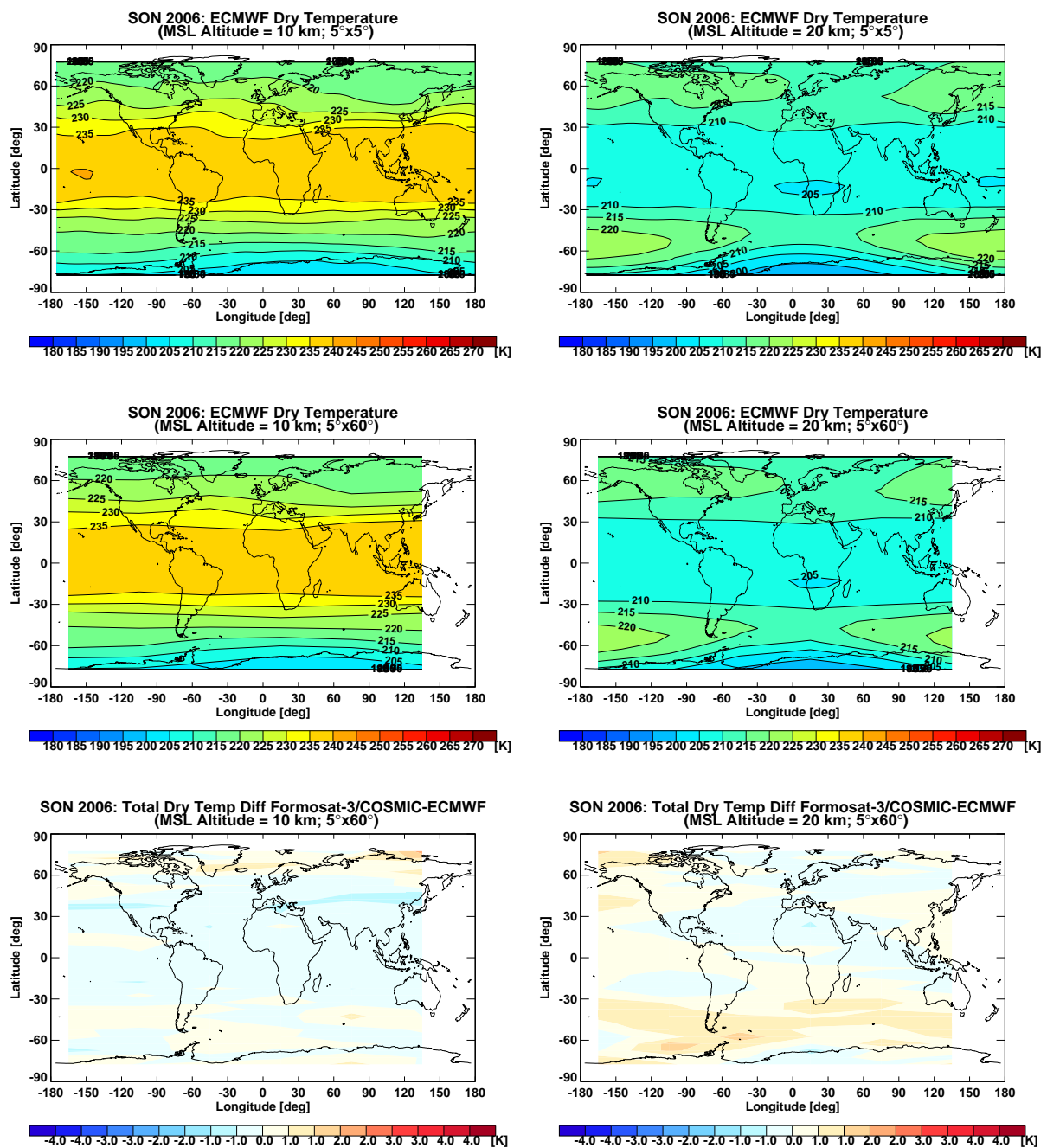


Figure 15: Latitude-longitude maps example for climate temperature monitoring, as possible in future with IASI profiles ingested into the CLIPS system, at different resolutions. Selected latitude vs. longitude example maps are shown at 10 km altitude (left column; "upper troposphere map") and at 20 km altitude (right column; "lower stratosphere map"), respectively. What is illustrated are high resolution ECMWF climatologies as "IASI-proxy" data (top row), coarser resolution ECMWF/"IASI-proxy" climatologies (middle row), and the difference between coarser resolution COSMIC climatologies from real profiles and the corresponding coarser resolution ECMWF/"IASI-proxy" climatologies (bottom row).

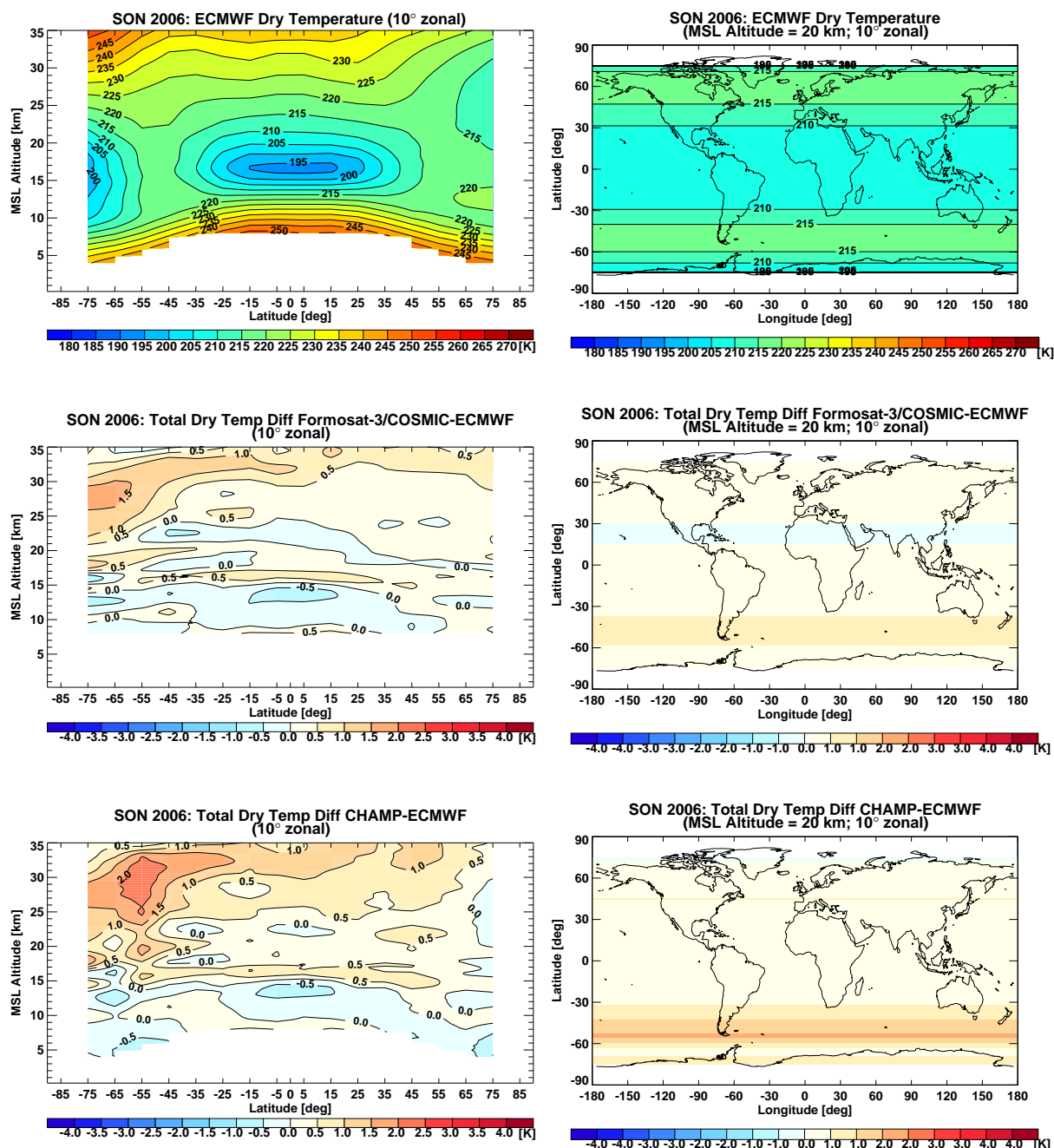


Figure 16: Zonal-band slices and maps example for climate temperature monitoring, as possible in future with IASI profiles ingested into the CLIPS system, at 10° zonal-band resolutions. A zonal-band slice example (left column) and a zonal-band map example at 20 km altitude (right column) is shown, respectively. What is illustrated are zonal-band ECMWF/"IASI-proxy" climatologies (top row), and the difference between zonal-band resolution COSMIC and CHAMP climatologies, both from real profiles, and the corresponding zonal-band resolution ECMWF/"IASI-proxy" climatologies (middle and bottom row, respectively).

4 Conclusions and Outlook

The first part of the report presents results of the initial validation based on a test orbit data set provided by EUMETSAT, ranging from April 2 to April 3, 2007. In terms of forward modeling the study was performed by utilizing the fast radiative transfer model RTIASI (*Matricardi and Saunders* (1999)). RTIASI was found to be suitable for the calculation of radiances and Jacobians for temperature, humidity, ozone, and SST for our purpose of a combined temperature, humidity, and ozone profile and SST retrieval from IASI spectra and it provides satisfactory forward model error characteristics. In terms of the retrieval algorithm and channel reduction procedures we used the algorithm and methods described in the enhancement report of this project (*Schwaerz et al.* (2007)).

We investigated the retrieval performance of this joint optimal estimation system based on a complete MetOp orbit of real IASI data, starting on April 2, 2007, at 23:20 UTC, and ending on April 3, 2007, at 0:23 UTC. We validated the IASI-derived dataset (clear-air profiles, i.e., those which passed cloudy profiles elimination) against co-located profiles from a high-resolution ECMWF atmospheric analysis of April 3, 2007, 0:00 UTC.

In general we found that the system provides profiles of temperature and humidity, which improve over the *a priori* profiles from an ECMWF 24h forecast throughout the retrieval domains of interest in the atmosphere. In the case of ozone, improvements were found especially in those stratospheric regions which exhibit high concentrations of this gas, i. e., around the peak of the atmospheric ozone layer, where rms errors were reduced to near 10% over *a priori* errors of 20%. The SST retrieval was not found as robust as in the simulation study but was still very accurate with rms errors at the sub-Kelvin level. Reasons for degraded performance to this end originate from limitations in realistic surface (emissivity) modeling and weaknesses in detection of clouds, i.e., an inclusion of partly cloudy pixels in the retrieval process and the non-detectability of low clouds by current cloud detection algorithms (c. f. *Lavanant and Lee* (2005)).

Weaknesses in retrieving atmospheric parameters occur specifically at levels where the sensitivity of the relevant weighting functions in the Jacobian matrix is limited, such as found in the simulation study. The sensitivity to SST is overall very good, thanks to the "atmospheric window" channels.

In comparing the joint multi-parameter retrieval to simplified single-parameter retrievals it was found that the joint processing significantly improves over the single-parameter retrieval, consistent with the results of the simulation study. This provided us with further confidence in the robustness and utility of the joint retrieval for future climate monitoring application, after the next steps of advancement such as in cloud detection and cloud clearing.

The results obtained from this initial validation also provided guidance for next and meanwhile on-going advancements, including a further improvement of the statistical model of the *a priori* uncertainties for temperature and humidity as well as the usage of the newest version of the forward model RTIASI, which contains a new scheme for prediction of the water vapor continuum, a refinement of the vertical pressure grid, an inclusion of some more trace gases as profile variables, an introduction of a solar term to evaluate the solar radiance reflected by a land or water surface (c. f. *Matricardi* (2003)) and an inclusion of clouds and aerosols (*Matricardi* (2004)). The updated processing system will also include a cloudy profiles elimination step in the system.

Overall the initial validation indicates that the IASI data hold — while still further processing improvements are needed for this very "young" dataset — high potential to significantly improve upon current operational satellite data for weather and climate applications.

On the prepared climatology processing of IASI-retrieved profiles, presented in the second part of the report, the developed Wegener Center climatology processing system (CLIPS) was tested with different representative datasets, including "IASI proxy" atmospheric profiles densely

sampled from ECMWF analysis fields and real radio occultation data, from which conclusions are reached as follows.

The Wegener Center CLIPS tool is prepared to ingest IASI-retrieved profiles similarly to radio occultation-retrieved profiles (e.g., from GRAS on MetOp; cf. *Pirscher et al.* (2007)).

The possible horizontal resolution of climatologies with IASI is higher than with radio occultation (e.g., GRAS), the latter being superior in the vertical resolution. Furthermore, the information gain on horizontal-geographical climate variability due to higher resolution of IASI has been well illustrated.

In summary, regarding the future promise of the European MetOp operational mission in this field, the combination of IASI and GRAS information is truly the method of choice. It is highly promising, as it allows, based on the complementary strengths of IASI and GRAS, for excellent climate monitoring at both high horizontal and vertical resolution scales.

Acknowledgments

The authors thank J. Fritzer, A. K. Steiner (WegCenter, Univ. of Graz, Austria), C. Retscher (ESA/ESRIN, Frascati, Italy), and A. Loescher (DMI, Copenhagen, DK) for many valuable discussions and advice during the processing system development, E. Weisz (SSEC, Univ. of Wisconsin, Madison, WI, USA) for fruitful discussions on retrieval methodology, P. Schluessel (EUMETSAT, Darmstadt, Germany) for providing the forward model RTIASI (which is a property of EUMETSAT) and the IASI level 1c noise values, X. Calbet (EUMETSAT) for providing valuable help in receiving the IASI test orbit data, and M. Matricardi (ECMWF, Reading, U. K.) for helpful advice related to RTIASI. The MetOp IASI test orbit data were provided by EUMETSAT under the ESA/EUMETSAT Research Announcement of Opportunity (RAO) Project GRASIVAL (ID 3057, PI G. Kirchengast). ECMWF provided access to atmospheric analyses and short term forecast fields. M. Schwaerz and M. Pock received financial support for the work from the MULTICLIM project funded by the Austrian Ministry for Traffic, Innovation, and Technology and managed under Contract No. ALR-OEWP-WV-326/06 of the Austrian Aeronautics and Space Agency (FFG-ALR).

List of References

- Camy-Peyret, C., and J. Eyre (1998), The IASI science plan, *ISSWG report*, CNES, Paris, France.
- ECMWF (2004), *IFS Documentation CY28r1*, European Centre for Medium-Range Weather Forecasts, Reading, UK.
- Foelsche, U., M. Borsche, A. K. Steiner, A. Gobiet, B. Pirscher, G. Kirchengast, J. Wickert, and T. Schmidt (2007), Observing upper troposphere-lower stratosphere climate with radio occultation data from the CHAMP satellite, *Clim. Dyn.*, doi:10.1007/s00382-007-0337-7.
- Lavanant, L., and A. C. L. Lee (2005), A global cloud detection scheme for high spectral resolution instruments, in *Proceedings of the Fourteenth International TOVS Study Conference*, pp. 149 – 160, Beijing, China.
- Liou, K. N. (2002), *An Introduction to Atmospheric Radiation (Second Edition)*, Elsevier Science (USA), Orlando.
- Matricardi, M. (2003), RTIASI-4, a new version of the ECMWF fast radiative transfer model for infrared atmospheric sounding interferometer, *ECMWF Technical Memorandum*, ECMWF, Research Department, Reading, U. K.
- Matricardi, M. (2004), The inclusion of aerosols and clouds in RTIASI, *Tech. Rep. Contract EUM/CO/02/989/PS*, ECMWF, Research Department, Reading, U. K.
- Matricardi, M., and R. Saunders (1999), A fast radiative transfer model for simulation of infrared atmospheric sounding interferometer radiances, *J. Appl. Optics*, *38*, 5679–5691.
- Pirscher, B., B. C. Lackner, M. Pock, I. Thaler, U. Foelsche, A. K. Steiner, and G. Kirchengast (2007), Initial validation of GRAS occultation data from MetOp and setup of regional climate monitoring including IPCC land and ocean regions, *Tech. Rep. for FFG-ALR No. 5/2007*, Wegener Center, Univ. of Graz, Austria.
- Schmetz, J., W. P. Menzel, C. Velden, X. Wu, L. van de Berg, S. Nieman, C. Hayden, K. Holmlund, and C. Gejo (1995), Monthly mean large scale analysis of upper troposphere humidity and wind field divergence derived from three geostationary satellites, *Bull. Amer. Meteor. Soc.*, *76*, 1578 – 1584.
- Schwaerz, M., M. Pock, and G. Kirchengast (2007), Advanced retrieval of atmospheric profiles and SST from IASI data, *Tech. Report for FFG-ALR No. 2/2007*, Wegener Center, Univ. of Graz, Austria.
- Spencer, R. W., and W. D. Braswell (1997), How dry is the tropical free troposphere? Implications for global warming theory, *Bull. Amer. Meteor. Soc.*, *78*, 1097 – 1106.
- Weisz, E. (2001), Temperature profiling by the Infrared Atmospheric Sounding Interferometer (IASI): Advanced retrieval algorithm and performance analysis (Ph. D. thesis), *Scientific Rep. 11*, IGAM, Institute of Physics, University of Graz, Austria.